ELSEVIER

Journal of Fluids and Structures 23 (2007) 1137–1148

JOURNAL OF FLUIDS AND STRUCTURES

www.elsevier.com/locate/jfs

Interactions between a rectangular cylinder and a free-surface flow

S. Malavasi*, A. Guadagnini

D.I.I.A.R., Politecnico di Milano, piazza Leonardo Da Vinci, 32, 20133 Milano, Italy

Received 31 May 2006; accepted 6 April 2007
Available online 18 June 2007

Abstract

The salient features of the interaction between a free-surface flow and a cylinder of rectangular cross-section are investigated and discussed. Laboratory-scale experiments are performed in a water channel under various flow conditions and elevations of the cylinder above the channel floor. The flow field is characterized on the basis of time-averaged and fluctuating local velocity measurements. Dynamic loadings on the cylinder are measured by two water-insulated dynamometers placed inside the cylinder structure. Starting from frequency and spectral analyses of the force signals, insights on the relationship between force dominant frequencies and the Strouhal number of the vortex shedding phenomenon are provided. Experimental results highlight the strong influence of the asymmetric configuration imposed by the two different boundary conditions (free surface and channel floor) on (i) the mean force coefficients and (ii) the vortex shedding frequencies. We provide an analysis of the nature of the dependence of average force coefficients on relevant dimensionless groups, i.e., the Reynolds number, normalized flow depth and cylinder submersion.

Keywords: Free-surface flow; Drag; Lift; Rectangular cylinder; Strouhal number

1. Introduction

The interaction between a rectangular cylinder and a flowing fluid has been the subject of several analyses [e.g. Naudascher (1991), Nakamura et al. (1991), Naudascher and Rockwell (1993), Simiu and Scanlan (1996), Rockwell (1998), and Hourigan et al. (2001)]. This type of flow configuration is relevant for many architectural and engineering technological applications, including the efficient design of buildings, bridges and other structures. Yet, the nature of several key issues, including the influence of asymmetric boundary conditions on the hydrodynamic loading on the structure still remains open to analysis and interpretation (Deniz and Staubli, 1997; Okajima et al., 1997; Hemon and Santi, 2002; Shimada and Ishihara, 2002).

Placement of a structure in a free-surface flow is a typical situation in which the dynamic loading is driven by an asymmetric boundary configuration. A relevant process which has been investigated experimentally is associated with the overflowing of river bridges. While some authors investigated this flow configuration focusing on specific bridge

*Corresponding author. Tel.: +39 2399 6261; fax: +39 2399 6298.
E-mail address: stefano.malavasi@polimi.it (S. Malavasi).

0889-9746/$ - see front matter © 2007 Elsevier Ltd. All rights reserved.
doi:10.1016/j.jfluidstructs.2007.04.002

deck structures [e.g. Tainsh (1965) and Denson (1982)], other studies modelled the bridge deck as a rectangular cylinder (Malavasi and Guadagnini, 2003; Malavasi et al., 2004; Picek et al., 2004).

In this context, Malavasi and Guadagnini (2003, 2005) provided experimental evidence on the nature of the dependence of the mean force coefficients on a normalized cylinder submersion, $h^* = (h - h_b)/s$ (where h is the water depth upstream of the obstacle, h_b is the bridge deck elevation above the channel floor and s is the thickness of the bridge deck) and on a deck Froude number, $\mathrm{Fr}_s = V/(gs)^{0.5}$ (where V is the mean upstream flow velocity and g is gravity). They pointed out that the actual values of the time-averaged force coefficients typical of a rectangular cylinder placed in an unbounded domain are dramatically different from those arising when the structure is placed in a free-surface flow. All their experiments were performed for a constant aspect ratio and elevation of the cylinder from the channel floor. Changing the upstream flow velocity and water depth, the authors found that (a) the drag coefficient attained values up to 3.4 and (b) the lift coefficient reached negative values up to -10.

Malavasi et al. (2004) used a Particle Image Velocimetry technique and provided physical depictions of the salient structures of the flow field around a rectangular bridge deck. They proposed a qualitative interpretation of the relationship between the flow field structures and the loading acting on the solid obstacle.

In a recent work, Cigada et al. (2006) documented and discussed the effects of an asymmetrical confined flow on a rectangular cylinder, placing the obstacle at various elevations from a solid wall within an open chamber wind tunnel. For several values of the Reynolds number and two values of the cylinder aspect ratio, they analysed the influence of the solid boundary on the time-averaged force coefficients and on the Strouhal number of the vortex shedding.

Here we focus on the hydrodynamic loading on a rectangular cylinder positioned in a steady-state free-surface flow. Three different sets of experiments are performed, as depicted in Fig. 1. These allow addressing the following key issues: the first test case (Fig. 1(a)) allowed to consolidate, improve and extend the results proposed by Malavasi and Guadagnini (2003); the second case (Fig. 1(b)) is aimed at analysing the influence of the relative distance of the cylinder from the boundaries (free surface and channel floor) for a given blockage ratio; and the third case (Fig. 1(c)) is targeted to ascertaining the effects of the elevation of the cylinder from the channel floor for a given cylinder submersion.

For these conditions, the nature of the interaction between fluid and structure is assessed by means of (a) the mean force coefficients and (b) the frequency analysis of the forces induced on the cylinder. This also allows investigating the Strouhal number associated with the vortex shedding mechanism.

Our analyses are based on the assumption that the cylinder is perfectly rigid and fastened. A discussion about experimental evidence supporting this assumption is presented in Section 3.2. This allows to associate the frequencies of the force induced on the cylinder with the frequencies of the vortex shedding mechanism.

The main parameters governing the interaction processes between a rigid and fastened rectangular cylinder and a steady-state unbounded flow include: (i) the cylinder aspect ratio, l/s (l and s, respectively, being the chord and the thickness of the rectangular cylinder); (ii) the Reynolds number, $\mathrm{Re} = (Vs)/\nu$ (where ν is kinematic viscosity); (iii) the inflow turbulent level, $\mathrm{Tu} = v'_{\mathrm{rms}}/V$ (where v'_{rms} and V are the standard deviation and the mean velocity of the flow along the dominant flow direction, respectively); (iv) the incidence angle, α, of V. The presence of asymmetrical boundary conditions in the flow scenario we investigate requires the introduction of additional controlling (dimensionless) groups. These include the normalized depth of the free-surface flow at some location upstream of the obstacle, h/s, and the normalized elevation of the obstacle from the channel floor, h_b/s. We provide a study of the main features associated with the cylinder excitation process upon setting l/s, Tu and α as constants in our experiments, while varying the remaining parameters.

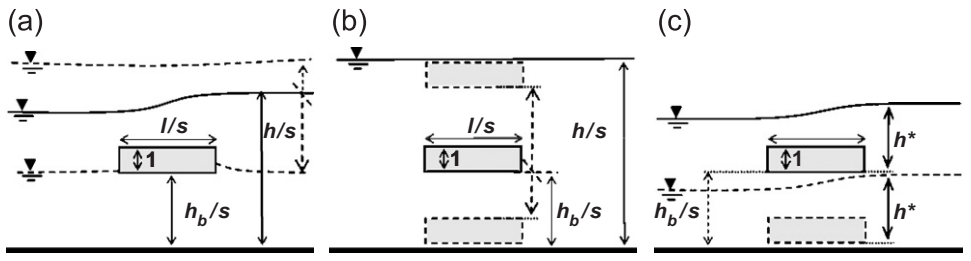

Fig. 1. Experimental conditions investigated: (a) l/s and h_b/s are constant and $0 < h/s < 8.5$; (b) l/s and h/s are constant and $0 < h_b/s < 6$; (c) l/s and h^* are constant and $0 < h/s < 3$. Here, s is the cylinder thickness, l is the length of the cylinder along the flow direction, h_b is the elevation from the channel floor, h is the water depth and $h^* = h/s - h_b/s$ is the dimensionless submersion of the cylinder.

We note that the dimensionless parameters Re and Fr_s are proportional when the fluid properties and gravity can be considered as constant. As opposed to Malavasi and Guadagnini (2003), we choose Re as the governing parameter instead of Fr_s, so that our results are readily comparable with those available in the literature.

The structure of the paper is as follows: Section 2 describes the experimental set-up; Section 3 is devoted to a discussion of the experimental results, which are analysed in terms of mean force coefficient on the cylinder (Section 3.1) and in terms of Strouhal number of the shedding frequency (Section 3.2). We then offer some conclusions in Section 4.

2. Experimental set-up

The experiments were performed in a 5.0 m long, nontilted, plexiglas flume with a cross-section of width $B = 0.5$ m and height $H = 0.6$ m.

Direct measurements of forces are performed by means of a pair of ad hoc insulated dynamometers. These were customized to work under wet conditions and were connected to an automatic data acquisition system (Cigada et al., 2001). The dynamometers were covered with a nonwatertight wooden structure, resulting in a cylinder of rectangular cross-section of length $l = 0.18$ m and height $s = 0.06$ m. As detailed in Fig. 2, the outer cover is sub-divided into three parts. Only the middle portion of the obstacle, which is 0.25 m wide and is labelled as "sensitive part", is connected to the dynamometers. Each dynamometer is connected to two measurement channels, resulting in a total of four acquisition channels recording the fluctuations in time of forces acting along the drag and lift directions.

Experiments were performed upon placing the model at several elevations from the channel floor, i.e., $0.0\,\text{m} < h_b \leqslant 0.36\,\text{m}$, and at a distance $d = 3.35$ m from the inlet section. The flow field was characterized by $1.2 \times 10^4 \leqslant \text{Re} \leqslant 3.7 \times 10^4$, corresponding to sub-critical conditions of the free-surface flow. The flow conditions were checked by means of flow rate, local velocity and free-surface level measurements at an upstream reference section located at a distance of 0.61 m from the obstacle. The volumetric flow rate was measured via a magnetic flow-meter with an estimated expanded uncertainty $u_Q = \pm 3 \times 10^5\,\text{m}^3/\text{s}$. The depth of the free surface was measured by means of

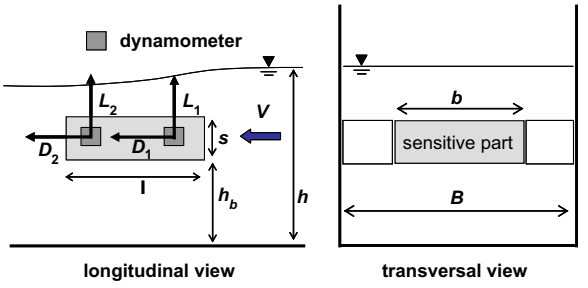

Fig. 2. Sketch of the experimental set-up.

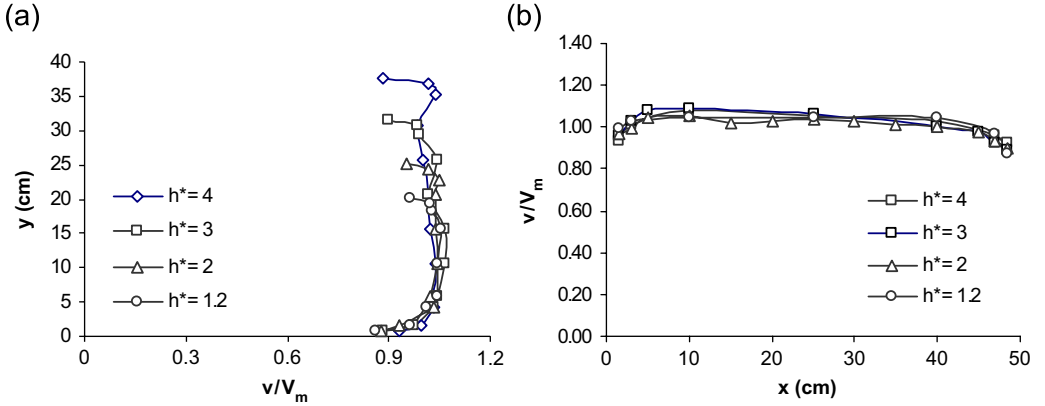

Fig. 3. Normalized velocity profiles at the reference section upstream of the cylinder for $\text{Re} = 2.00 \times 10^4$ (v is the local time-averaged velocity; V_m is the mean of v along a profile).

piezometer tubes (estimated expanded uncertainty $u_h = \pm 10^{-3}$ m). An average water level was obtained by taking three measurement points across the measurement cross-section. Details about the inflow velocities are provided by means of an impeller flow-meter (0.007 m diameter and declared uncertainty $u_v = 1\%$), which was used to characterize the velocity distribution of the flow along the horizontal and vertical directions. Fig. 3 depicts examples of the vertical and horizontal mean velocity profiles of free-surface flows at the above-mentioned reference section. Vertical profiles are measured in the middle of the water channel, whereas the horizontal profiles are measured at the cylinder elevation. The influence of the obstacle on the water level and on the velocity distribution at this section was negligible for the experiments performed.

The impeller flow-meter was also used to estimate the turbulence level of the flow. The turbulence level along the main flow direction, Tu, was calculated on the basis of a continuous acquisition (total acquisition time of 2 min). A value of Tu $\approx 14\%$ was obtained for the experimental range investigated.

Preliminary tests allowed to identify the parameters to be used in the data acquisition process (i.e., sampling frequency and total acquisition time) in order to adequately characterize the forces acting on the structure. Force data acquired at a 100 Hz frequency displayed good stability of the computed mean and variance within 2 min from the beginning of the acquisition process. The force acquisition tests are set on a standard total acquisition time of 20 min. Frequency analysis was performed via the power spectral density (PSD) of the signal, which was calculated according to the Welch method.

3. Results

We have considered the three sets of experimental conditions depicted in Fig. 1.

As discussed in Section 1, the first series of tests has been inspired by the results of Malavasi and Guadagnini (2003), where the problem of the hydrodynamic loading on a river bridge was investigated upon modelling the bridge deck as a rectangular cylinder (Fig. 1(a)). Our upgraded experimental set-up allowed first a thorough reproducibility check of the experiments of Malavasi and Guadagnini (2003), then an extension of the available experimental database, and finally the investigation of the main vortex shedding characteristics by means of the frequency analysis of the force data.

In the second series of experimental conditions, the normalized free-surface level at the reference upstream section is set to the value $h/s = 7$ and experiments are performed for various elevations of the cylinder from the channel floor (Fig. 1(b)).

Finally, the last series of tests is characterized by a constant value of the dimensionless submersion of the cylinder, i.e., $h^* = 5$, while placing the cylinder at various elevations from the channel floor (Fig. 1(c)).

In the following sections, we present our results and discuss the effects of the free-surface flow on the cylinder by focusing on (a) the analysis of the mean force coefficients and (b) the spectral analysis of the forces induced on the cylinder. The latter allowed investigating the Strouhal numbers associated with the characteristic frequencies of the process.

3.1. Force coefficients

According to the set-up employed for the force measurements, the lift and drag force coefficients, respectively, labelled as C_L and C_D, can be defined as

$$C_L = \frac{2(L_1 + L_2)}{\rho V^2 bs}, \qquad C_D = \frac{2(D_1 + D_2)}{\rho V^2 bs}, \tag{1,2}$$

where D_i and L_i ($i = 1, 2$) are the drag and the lift components of the loading acting on the ith dynamometer, ρ is fluid density and b is the transverse dimension of the sensitive portion of the cylinder of thickness s. We recall that C_L and C_D appearing in Eqs. (1) and (2) are computed on the basis of the frontal area of the cylinder, $b \times s$, also for experiments where the cylinder is only partially submerged, i.e., $h^* < 1$.

Fig. 4 depicts the results of the first series of experimental runs, corresponding to the geometrical setting of Fig. 1(a). The measured drag and lift coefficients confirm the behaviour discussed by Malavasi and Guadagnini (2003, 2005). Slight differences between the measured values and those reported by Malavasi and Guadagnini are mainly related to the upgrading of the experimental set-up. Uncertainty associated with measurements of state variables of interest has been analysed by means of the same methodology used by Malavasi and Guadagnini (2003).

Fig. 4 highlights that both force coefficients strongly depend on Re within the range $1 \leqslant h^* \leqslant 4$. Two distinct behaviours can be recognized within this range: (a) when Re lies within an interval $1.2 \times 10^4 \leqslant \mathrm{Re} \leqslant 2.0 \times 10^4$, data

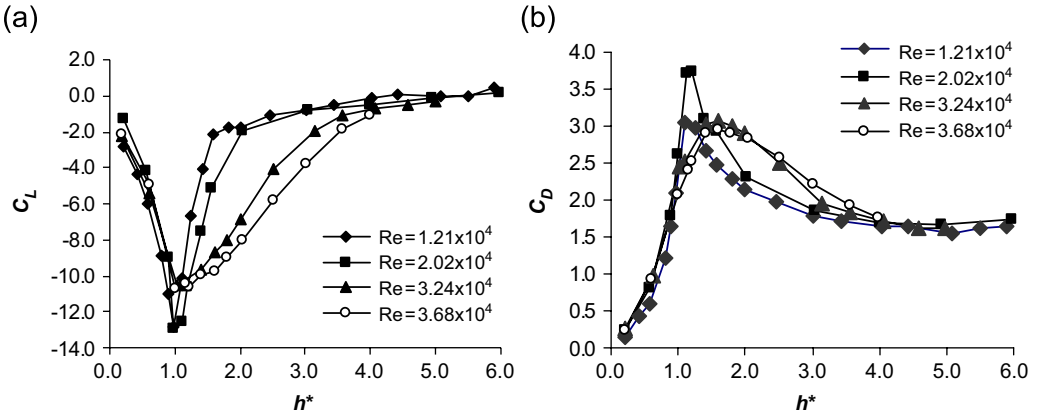

Fig. 4. Mean force coefficients for case (a) of Fig. 1 ($h_b/s = 2.33$).

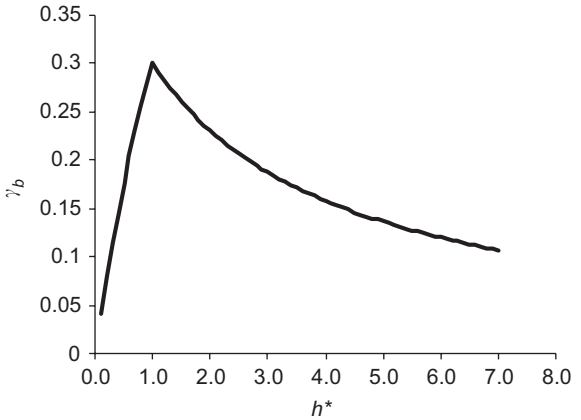

Fig. 5. Dependence of the blockage ratio ($\gamma_b = s/h$) on h^* for the data reported in Fig. 4 ($h_b/s = 2.33$).

display a sharp, high peak after which the absolute values of the coefficients decrease quickly towards asymptotic values as h^* increases; (b) for $\mathrm{Re} \geqslant 3.0 \times 10^4$, the force coefficients display a smoother dependence on h^* and tend to the same asymptotic values attained for low Re as h^* increases. The drag coefficient asymptotically tends to a value which is larger than that indicated in the literature for unbounded flow conditions (Simiu and Scanlan, 1996; Shimada and Ishihara, 2002; Noda and Nakayama, 2003). The lift coefficient asymptotically tends to zero.

Upon considering the depictions of the velocity field structure in the cases of unbounded [e.g. Naudascher and Wang (1993), Deniz and Staubli (1997), and Yu and Kareem (1998)] and free-surface (Malavasi et al., 2004) flows, the observed behaviour of C_L can be interpreted as follows. The average dynamic pressure distribution on the two horizontal sides of the cylinder is connected with the average size of the formation bubbles generated by flow detachment at the leading edges of the obstacle; under unbounded flow conditions the boundary conditions of the system are symmetric and the sizes of the bubbles on the upper and bottom faces of the cylinder coincide ($C_L = 0$). On the contrary, the presence of asymmetrical boundary conditions cause the relative size of the detachment bubbles to differ so that a nonzero lift coefficient is detected. When $0 \leqslant h^* < 1$, the liquid flows under the cylinder and flow separation occurs at the bottom side of the cylinder. Increasing h^* in this flow configuration produces a corresponding increase of the size of the separation bubble developing at the bottom upstream leading edge of the cylinder. As a consequence, the (negative) pressure values acting on the bottom side of the cylinder increase. Since the upper side of the cylinder is subject to atmospheric pressure, the (negative) lift increases with h^*. When $h^* \geqslant 1$ the cylinder is completely submerged. This implies that the size of the separation bubble which develops at the upper upstream leading edge of the cylinder might equilibrate the pressure distribution along the bottom side of the cylinder. Therefore, the lift component increases with h^*.

The behaviour of the drag coefficient is difficult to interpret solely on the basis of qualitative arguments about the structure of the flow field around the obstacle. The peak displayed by C_D (Fig. 4(b)) can be explained by considering the influence of the blockage ratio, $\gamma_b = s/h$ (i.e., the ratio between the thickness of the cylinder and the depth of the fluid stream at the reference section) when, as in our case, the channel has a rectangular cross-section. Fig. 5 suggests that variations of h^* induce variations of the blockage ratio. The increase of γ_b with h^*, observed for $0 \leqslant h^* \leqslant 1$, causes (i) a local increase of the velocity in the wake of the obstacle and (ii) a subsequent increase of the pressure drop on the rear face of the cylinder, thus increasing the drag coefficient. A further increase of h^* results in a reduction of γ_b. On the other hand, the presence of a free surface and the fact that distortions in the shape of the free surface occur mainly in the proximity of the obstacle do not allow a direct comparison of the effect of the blockage ratio in this context with evidences typical of aerodynamics applications (Simiu and Scanlan, 1996; Okajima et al., 1997). The presence of a free surface is actually the element which causes the strong dependence of the force coefficients on Re observed in our experimental conditions for $0.8 < h^* < 4$. This dependence is usually not observed for unbounded flows (Naudascher, 1991; Simiu and Scanlan, 1996; Deniz and Staubli, 1997; Cigada et al., 2006). The back-watering effects which are typical of free-surface flows depend on Re and are relevant in the range of h^* were investigated. To illustrate the point, Fig. 6 presents pictures taken for two different submersion levels of the obstacle and documenting how Re affects the free-surface behaviour around the cylinder. For $\mathrm{Re} = 1.2 \times 10^4$, the geometric distortion of the free surface of the flow close to the cylinder is negligible. A significant distortion of the free surface is displayed in Fig. 6 for $\mathrm{Re} = 3.7 \times 10^4$. In order to satisfy the mass balance requirement, the free-surface modification involves an increase of the differences between the upstream velocities at the reference section and the velocities around the obstacle. This is especially clear in the case of $h^* = 2$. Therefore, an increase of the drag coefficient can be attributed to the magnification of the pressure drop between the front and the rear face of the cylinder.

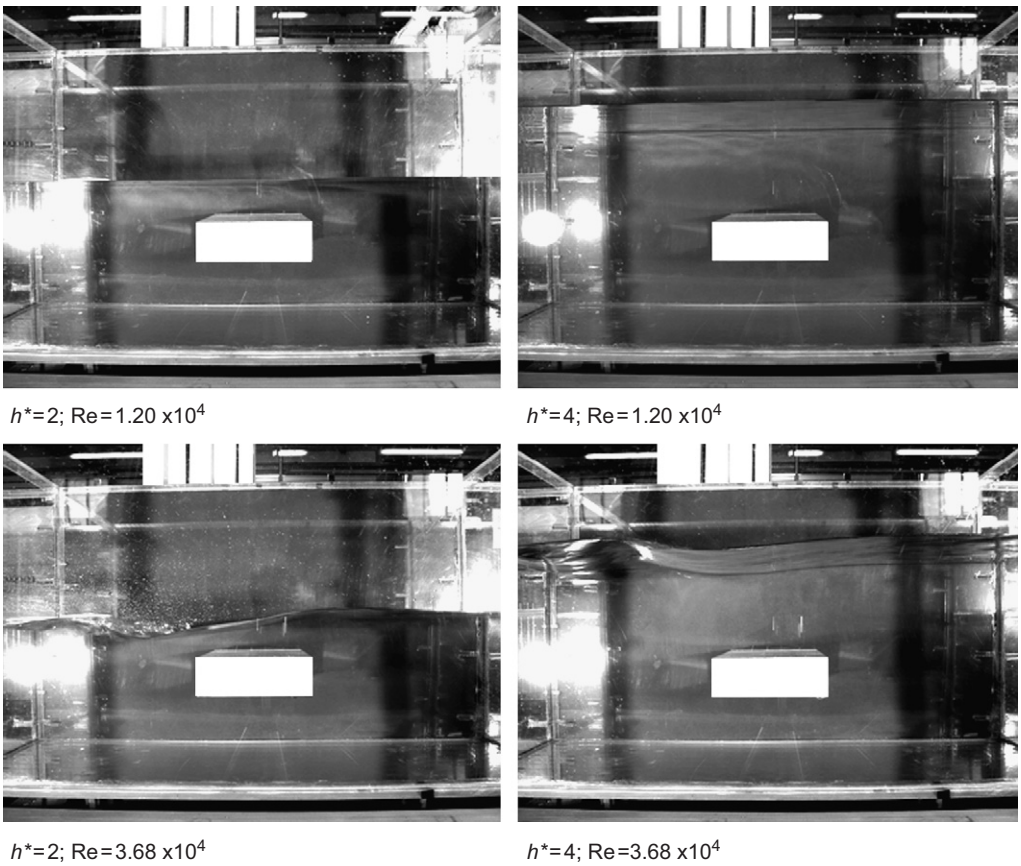

Fig. 6. Local distortions of the pattern of the free surface of the flow in the proximity of the structure.

The experimental evidence of Figs. 4 and 6 suggests that the blockage ratio and the presence of the free surface jointly affect the loading on the cylinder. With the aim of separating these two effects, we analyse the results of a tests performed upon changing the cylinder elevation while keeping a constant blockage ratio (Fig. 1(b)).

Fig. 7(a) illustrates the dependence of C_L on h^*. Upon reducing the cylinder elevation, h_b, while keeping a constant water depth, the submersion of the cylinder increases. Since the flow separation mechanism appears on both of the horizontal sides of the cylinder, the (absolute) value of C_L tends to vanish, thus recovering a scenario where the influence of the boundary surfaces is negligible. This is observed for $4 \leqslant h^* \leqslant 6$. A further increase of the cylinder submersion, i.e., $h^* > 6$, results in a significant influence of the channel floor. The latter causes the lift coefficient to increase up to a value $C_L \approx 3$, which is recovered when $h_b = 0$, i.e., the cylinder is positioned on the channel floor. This scenario, corresponding to $h^* = 7$, was obtained by placing the cylinder at an elevation of about 1 mm above the channel floor, to allow a proper measurement of the lift force. The effects of the boundaries (free surface and channel floor) are less significant on C_D, as revealed in Fig. 7(b), where the trend of C_D with h^* is not as evident as in the case of C_L.

Upon comparing values of C_L of Fig. 4 and Fig. 7, one notes that these coincide for $h^* = 5$ ($C_L \approx 0$) independently of Re. The same can be observed with reference to the values of C_D ($C_D \approx 1.6$). Reducing the structure submersion while varying γ_b (Fig. 4) results in a strong dependence of both C_L and C_D on Re. On the other hand, C_L and C_D are not affected by Re when γ_b is kept constant (Fig. 7). We also note that the qualitative behaviour of the force coefficients evidenced in Fig. 7 for $h^* \geqslant 5$ is consistent with previous results of Cigada et al. (2006), albeit in a wind channel.

The third series of experiments, where the cylinder submersion is fixed while varying the elevation of the cylinder above the channel floor, supports the findings previously described. As an example, Fig. 8 shows the results

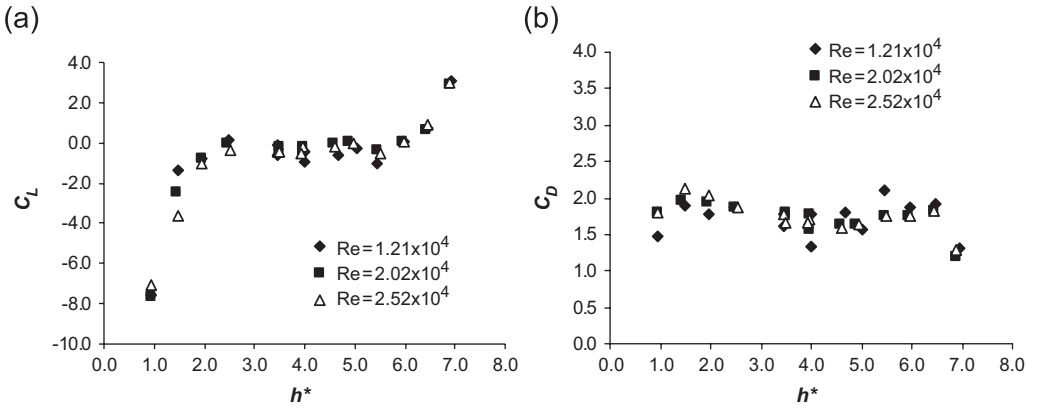

Fig. 7. Mean force coefficients for case (b) of Fig. 1 ($h/s = 7$).

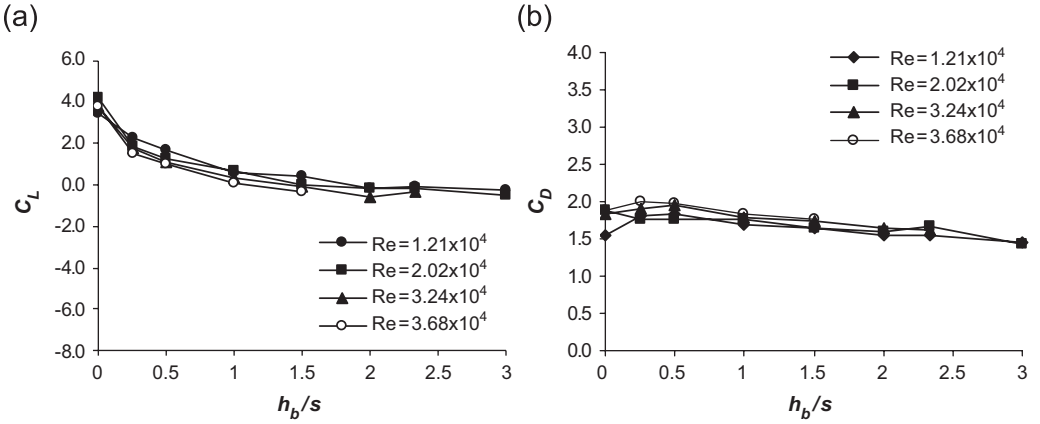

Fig. 8. Dependence of the force coefficients on h_b/s and Re for $h^* = 5$ (case (c) of Fig. 1).

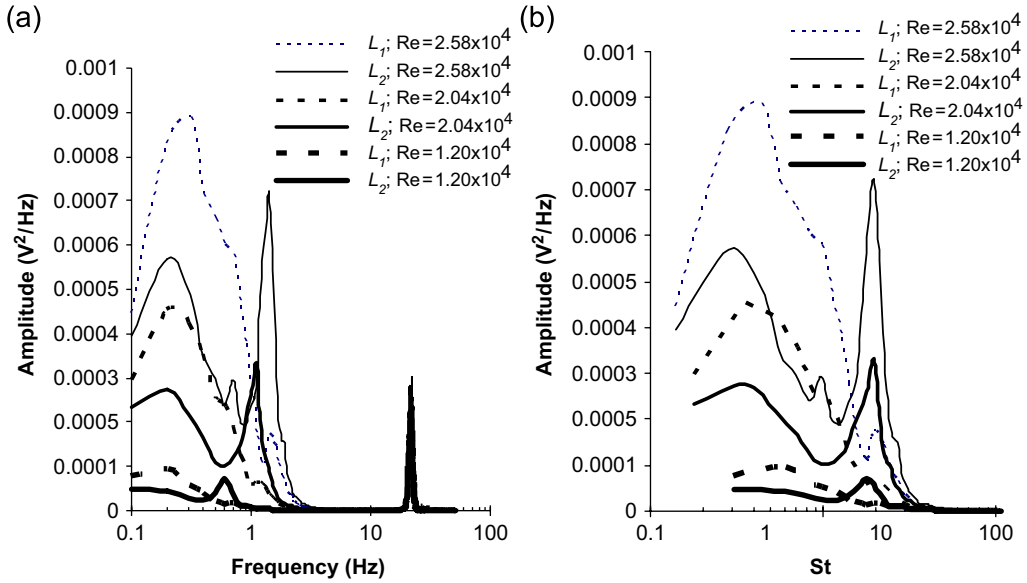

Fig. 9. Power spectra of the lift components (L_1, L_2) on the cylinder for $h_b/s = 3$: (a) amplitude versus frequency; (b) amplitude versus Strouhal number.

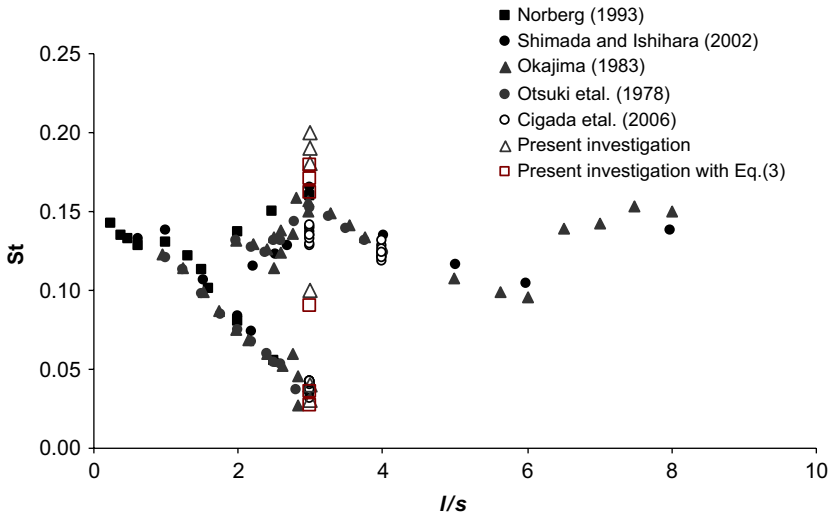

Fig. 10. Strouhal number (St) of vortex shedding for a rectangular cylinder in a cross-flow. Norberg (1993): $\mathrm{Re} = 1.3 \times 10^4$, $\mathrm{Tu} < 0.06\%$, $\gamma_b < 0.05$; Shimada and Ishihara (2002): numerical simulations; Okajima (1983): $\mathrm{Re} = 4.2 \times 10^4$, $\mathrm{Tu} = 0.4\%$, $\gamma_b = 1\%$—from Shimada and Ishihara (2002); Otsuki et al. (1978): $\mathrm{Re} = 6.5\text{–}7.6 \times 10^4$, $\mathrm{Tu} = 0.2\%$, $\gamma_b = 5.4\%$—from Shimada and Ishihara (2002); Cigada et al. (2006): $\mathrm{Re} = 0.8\text{–}3.7 \times 10^4$, $\mathrm{Tu} = 7\text{–}1\%$, $\gamma_b = 4.4\%$; present investigations: $\mathrm{Re} = 1.2\text{–}2.6 \times 10^4$; $\mathrm{Tu} = 14\%$; $\gamma_b = 14.3\%$.

corresponding to a case with the relatively large value of submersion $h^* = 5$. This condition ensures that the effects of the blockage ratio do not sensibly affect the behaviour of the data upon varying Re. Direct comparison of the data of Figs. 7 and 8 suggests that a reduction of the blockage ratio produces a significant increase of the lift coefficient (note that $h_b/s = 0$ corresponds to $h/s = h^* = 5$). As previously discussed, the influence of the blockage ratio is less relevant on C_D than on C_L.

3.2. Shedding frequencies

This section is devoted to the frequency analysis of the lift components induced by the free-surface flow on the rectangular cylinder. Due to the positioning of the dynamometers, the lift channels are more sensitive to the vortex shedding excitation than the drag channels.

Fig. 9(a) shows the frequency distribution of the two components of the lift acting on the cylinder. The experimental conditions analysed have been chosen on the basis of the results of Fig. 7(a), within a range of parameters for which the lift coefficient is not significantly affected by the boundaries (i.e., $h^* = 4$; $h_b/s = 3$; $\mathrm{Re} = 1.20 \times 10^4$, 2.04×10^4, 2.58×10^4). The peaks displayed by all data sets at the frequency of about 21 Hz identify the resonance frequency of the cylinder along the lift direction. This frequency value has also been recovered during a series of preliminary tests and is clearly distinguishable from the vortex shedding frequencies which are less than 10 Hz in the entire range of parameters investigated.

Fig. 9(b) depicts the dependence of the data of Fig. 9(a) on the Strouhal number within the range of St values where the vortex shedding effects are included. Here, we note that all L_2 data are characterized by sharp peaks occurring at

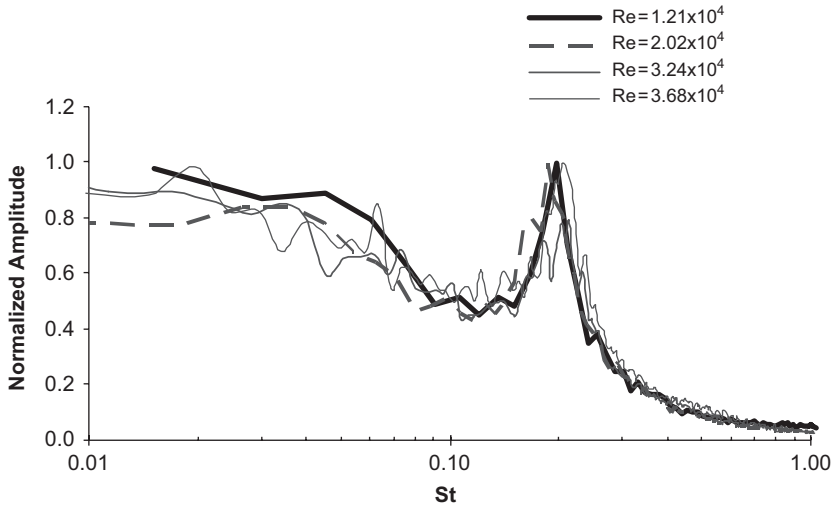

Fig. 11. Normalized spectra of the lift component L_2 for various Re and $h^* = 4$ and $h_b/s = 2.33$.

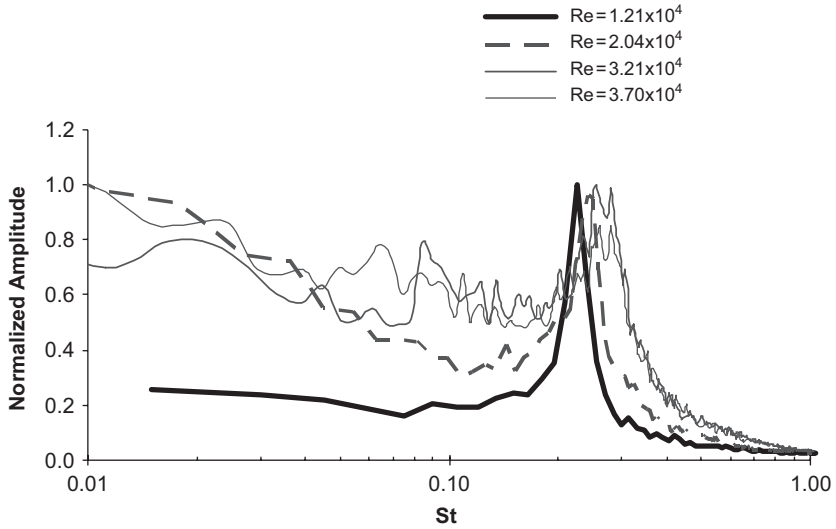

Fig. 12. Normalized spectra of the lift component L_2 for various Re and $h^* = 2$ and $h_b/s = 2.33$.

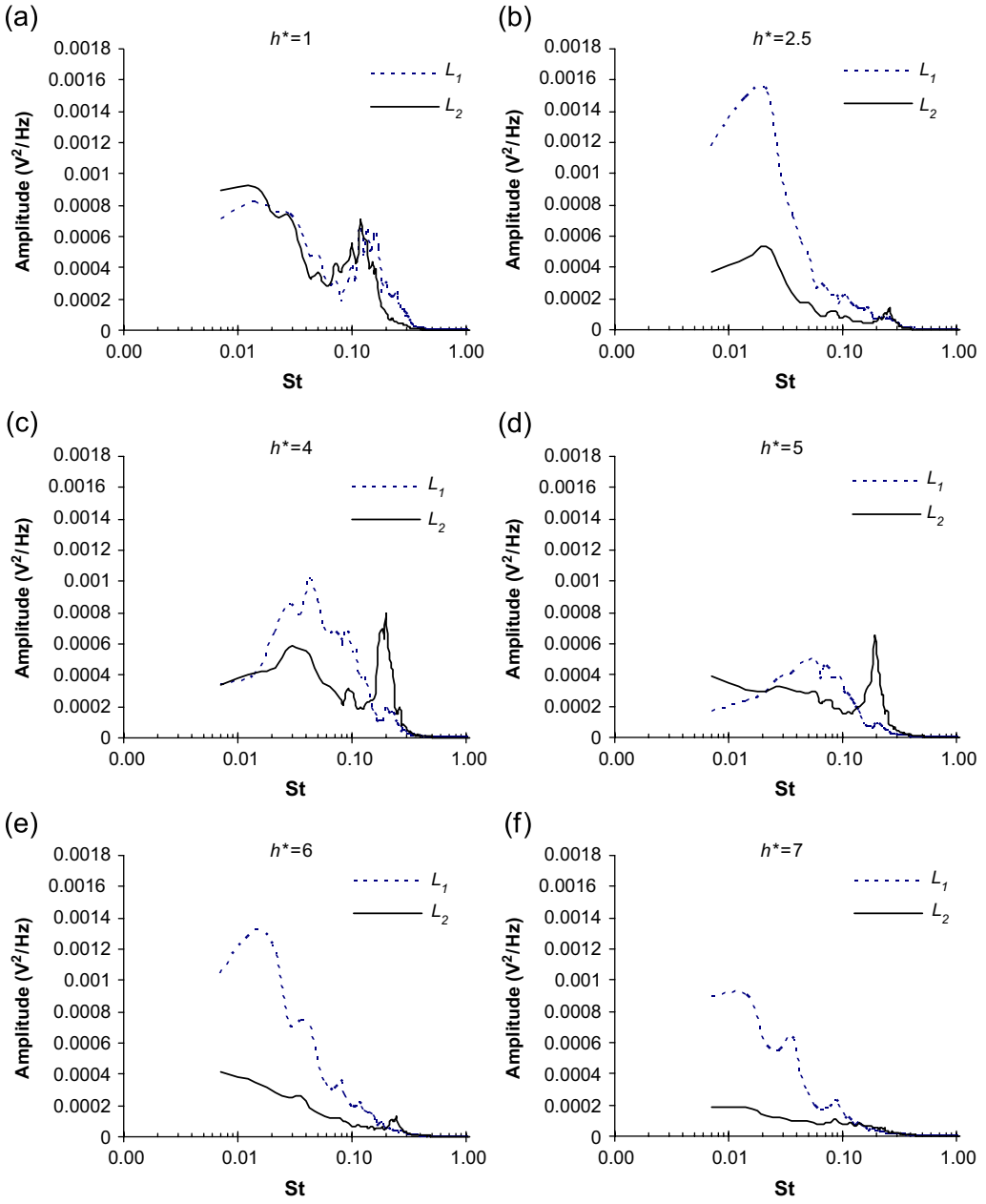

Fig. 13. Power spectra of the lift components L_1 and L_2 for various h^* ($\mathrm{Re} = 2.5 \times 10^4$ and $h/s = 7.0$).

$\mathrm{St} \approx 0.20$ and other peaks for $\mathrm{St} < 0.20$. These are also distinguishable on the channel L_1. They do not identify a unique Strouhal number and are linked to the frequency of the formation bubbles. For $\mathrm{Re} = 2.58 \times 10^4$, a third peak starts appearing at $\mathrm{St} \approx 0.1$. Its presence is consistent with the findings of Naudascher and Wang (1993), who emphasized that multiple shedding frequencies might coexist for the aspect ratio considered.

Fig. 10 compares our data with those of several other authors, who analysed the dependence of the Strouhal number typical of vortex shedding phenomena for a rectangular cylinder placed in unbounded cross-flow on the aspect ratio, l/s.

In order to produce a meaningful comparison, we have also corrected our data by means of the procedure suggested by Okajima et al. (1997):

$$\mathrm{St}_c = \mathrm{St}(1 - \gamma_b)^n, \tag{3}$$

where n is an experimental coefficient ($n = 0.7$ for $l/s = 3$). Eq. (3) has been proposed for situations where the flow field is confined between solid walls. However, when the free surface is not disturbed by the presence of the structure (i.e., as in the case of large submergence ratios) the blockage effects do not deviate significantly from those encapsulated in Eq. (3).

The shedding frequencies obtained from our experiments are consistent with those of other authors, even though the turbulent intensities of flow, Tu, in our tests are about an order of magnitude larger than those which were found for the literature data reported in Fig. 10.

In order to analyse the influence of the distortion of the free surface on the vortex shedding frequencies, Figs. 11 and 12 depict the frequency analysis of the lift channel L_2 for $h^* = 4$ and 2, respectively, in terms of a normalized amplitude. The latter has been calculated as the ratio between the signal amplitude and the maximum amplitude recorded.

Fig. 11 reveals that varying Re when $h^* = 4$ does not significantly affect the frequency distribution and the value of the dominant frequency of the lift channel L_2. These results suggest that the vortex shedding phenomenon does not change significantly with Re within the investigated range, even though we note an increase of dispersion of the dominant frequencies when Re increases from 3.24×10^4 to 3.68×10^4. Contrariwise, one can note that the dominant frequency of the lift channel L_2 significantly changes with Re for $h^* = 2$ (Fig. 12).

Key features revealed by Fig. 12 include the increase of the Strouhal number corresponding to the dominant frequency and an increase of frequency dispersion that causes a reduction of the relative energy content of the trailing-edge vortex shedding (TEVS). These results evidence differences on the flow structures in the wake region and are in general agreement with the differences on the drag and lift coefficients observed in Fig. 4 for different Re.

Fig. 13 compares the frequency distributions of the two lift components, L_1 and L_2, measured for the second series of experiments, corresponding to the geometric setting of Fig. 1(b). These results document the dependence of the shedding frequencies on h^*, in the range $1 \leqslant h^* \leqslant 7$, when $\mathrm{Re} = 2.5 \times 10^4$ and $h/s = 7$. When $h^* = 1$, L_1 and L_2 display similar behaviours (Fig. 13(a)). Under this condition the separation bubble which is formed at the bottom upstream leading edge of the obstacle spans the entire chord of the cylinder (Malavasi et al., 2004), so that similar excitations are induced on the two dynamometers. When the cylinder submersion increases, the two lift channels evidence different behaviours and two distinct dominant frequencies are clearly distinguishable (Fig. 13(b)). This difference between the signals of the two lift channels is clear when $h^* = 4$ (Fig. 13(c)). In this particular situation which mimics symmetric flow conditions, the two vortex shedding mechanism of leading-edge vortex shedding (LEVS) and trailing-edge vortex shedding (TEVS) are well distinguishable.

The dominant frequencies observed for $h^* = 4$ (Fig. 13(c)) are recovered for $h^* = 5$ (Fig. 13(d)), in agreement with what evidenced for the behaviour of C_L (Fig. 7). When $h^* = 6$, the effects of the channel floor become relevant (Fig. 13(e)) and the amplitude of the dominant frequencies on L_2 is significantly reduced, while low frequencies become relevant on L_1.

4. Conclusions

The dynamic interactions between a rectangular cylinder and a free-surface flow are significantly different from those observed in unbounded flows or in-flow fields governed by the presence of solid boundaries. The two key features which need to be considered are the asymmetry of the flow field and the distortion of the free surface. These aspects have been investigated in terms of their effects on the mean drag and lift coefficients, spectral analysis of the dynamic loading on the cylinder and Strouhal number of the vortex shedding for the case of a cylinder with an aspect ratio $l/s = 3$. Three series of experiments have been performed (see Fig. 1 for a sketch of the settings adopted) to extend the results proposed by Malavasi and Guadagnini (2003) and address the influence of the relative position of the cylinder between the boundaries (free surface and channel floor). Our work leads to the following major conclusions.

(1) The effects of the asymmetry of the flow condition have a profound impact on the lift coefficient while a limited influence is observed on the drag coefficient (Figs. 4 and 7). Figs. 7 and 13 document that the dynamic excitation of the cylinder, expressed in terms of mean force coefficients and dominant frequency of vortex shedding, is clearly influenced by the relative (vertical) distance between the structure and the channel floor and the free surface of the flow.
(2) The distortion of the free surface in the proximity of the structure is responsible for the dependence of the force coefficients on the Reynolds number. This is usually not observed in unbounded or solid bounded flows in the range of Re investigated. The occurrence of free-surface distortions is mainly due to the back-watering phenomenon,

which in turn depends on Re. A strong dependence of the force coefficients, C_L and C_D, on Re is highlighted for $0.8 < h^* < 4$ (Fig. 4). Significant effects of the presence of the free surface are also revealed on the vortex shedding frequency. This is clearly shown in Fig. 12, documenting the increase of the dominant vortex shedding frequency with Re.

(3) Our results suggest that the blockage ratio and the presence of a free surface jointly affect the loading on the structure. We found that the effects of the blockage ratio are less relevant on C_D than on C_L, also in the presence of negligible distortion of the free surface close to the structure.

References

Cigada, A., Malavasi, S., Vanali, M., 2001. Direct forces measurement on a submerged bridge model. In: Proceedings of the First International Conference on Fluid Structure Interaction, 26–28 September, Halkidiki, Greece, pp. 305–314.

Cigada, A., Malavasi, S., Vanali, M., 2006. Effects of an asymmetrical confined flow on a rectangular cylinder. Journal of Fluids and Structures 22, 213–227.

Deniz, S., Staubli, Th., 1997. Oscillating rectangular and octagonal profiles: integration of leading- and trailing-edge vortex formation. Journal of Fluids and Structures 11, 3–31.

Denson, K.H., 1982. Steady-state drag, lift and rolling-moment coefficients for inundated inland bridges. Report MSHD-RD-82-077, National Technical Information Service, Springfield, VA.

Hemon, P., Santi, F., 2002. On the aeroelastic behavior of rectangular cylinder in cross-flow. Journal of Fluids and Structures 16, 855–889.

Hourigan, K., Thompson, M.C., Tan, B.T., 2001. Self-sustained oscillation in flows around long blunt plates. Journal of Fluids and Structures 15, 387–398.

Malavasi, S., Guadagnini, A., 2003. Hydrodynamic load on river bridge. Journal of Hydraulic Engineering 129, 854–861.

Malavasi, S., Guadagnini, A., 2005. Closure to "Hydrodynamic loading on river bridges" by Stefano Malavasi and Alberto Guadagnini. Journal of Hydraulic Engineering 131, 622–623.

Malavasi, S., Franzetti, S., Blois, G., 2004. PIV investigation of flow around submerged river bridge. In: Proceedings of the International Conference River Flow 2004, Napoli, Italy, pp. 601–608.

Nakamura, Y., Ohya, Y., Tsuruta, H., 1991. Experiments on vortex shedding from flat plates with square leading and trailing edges. Journal of Fluid Mechanics 222, 437–447.

Naudascher, E., 1991. AIRH Design Manual: Hydrodynamic Forces. A.A. Balkema Publishers, Rotterdam.

Naudascher, E., Rockwell, D., 1993. AIRH Design Manual: Flow Induced Vibrations—An Engineering Guide. A.A. Balkema Publishers, Rotterdam.

Naudascher, E., Wang, Y., 1993. Flow-induced vibrations of prismatic bodies and grids of prisms. Journal of Fluids and Structures 7, 341–373.

Noda, H., Nakayama, A., 2003. Free-stream turbulence effects on the instantaneous pressure and forces on cylinders of rectangular cross section. Experiments in Fluids 34, 332–344.

Norberg, C., 1993. Flow around rectangular cylinders, pressure forces and wake frequencies. Journal of Wind Engineering and Industrial Aerodynamics 49, 187–196.

Okajima, A., Yi, D., Kimura, S., Kiwata, T., 1997. The blockage effects for an oscillating rectangular cylinder at moderate Reynolds number. Journal of Wind Engineering and Industrial Aerodynamics 69–71, 997–1011.

Picek, T., Havlik, A., Mattas, D., 2004. Pressure flow and overflow bridges. Journal of Hydrology and Hydromechanics 52, 185–192.

Rockwell, D., 1998. Vortex–body interactions. Annual Review of Fluid Mechanics 30, 199–229.

Shimada, K., Ishihara, T., 2002. Application of modified k–e model to the prediction of aerodynamic characteristics of rectangular cross section cylinders. Journal of Fluids and Structures 16, 465–485.

Simiu, E., Scanlan, R.H., 1996. Wind Effects on Structures. Wiley, New York.

Tainsh, J., 1965. Investigation of forces on submerged bridge beams. Report No. 108, Department of Public Works, University of New South Wales, Sydney, Australia.

Yu, D., Kareem, A., 1998. Parametric study of flow around rectangular prisms using LES. Journal of Wind Engineering and Industrial Aerodynamics 77–78, 653–662.